J|A|C|S
ARTICLES
Published on Web 02/28/2007

The Case of the Missing Ring: Radical Cleavage of a Carbon−Carbon Bond and Implications for GFP Chromophore Biosynthesis

David P. Barondeau,† Carey J. Kassmann, John A. Tainer, and Elizabeth D. Getzoff*

Contribution from the Department of Molecular Biology, The Skaggs Institute for Chemical Biology, The Scripps Research Institute, 10550 North Torrey Pines Road, La Jolla, California 92037

Received June 6, 2006; E-mail: edg@scripps.edu

Abstract: The green fluorescent protein (GFP) creates its fluorophore by promoting spontaneous peptide backbone cyclization and amino acid oxidation chemistry on its own Ser65, Tyr66, Gly67 tripeptide sequence. Here we use high-resolution crystallography and mutational analyses to characterize GFP variants that undergo backbone cyclization followed by either anticipated chromophore synthesis via Y66F Cα−Cβ double-bond formation or unprecedented loss of a Y66F benzyl moiety via Cα−Cβ bond cleavage. We discovered a Y66F cleavage variant that subsequently incorporates an oxygen atom, likely from molecular oxygen, at the Y66 Cα position. The post-translational products identified from these Y66F GFP structures support a common intermediate that partitions between Cα−Cβ oxidation and homolytic cleavage pathways. Our data indicate that Glu222 is the branchpoint control for this partitioning step and also influences subsequent oxygen incorporation reactions. From these results, we propose mechanisms for Y66F Cα−Cβ cleavage, oxygen incorporation, and chromophore biosynthesis with shared features that include radical chemistry. By revealing how GFP and RFP protein environments steer chemistry to favor fluorophore biosynthesis and disfavor alternative reactivity, we identify strategies for protein design. The proposed, common, one-electron oxidized, radical intermediate for post-translation modifications in the GFP family has general implications for how proteins drive and control spontaneous post-translational chemical modifications in the absence of metal ions.

Introduction

A surprising and critical finding of the Human Genome Project is that about 23 000−40 000 genes produce significantly more than 90 000 proteins.[1] This huge increase in protein diversity is created primarily by alternative gene splicing and protein post-translational modification (PTM). PTMs include proteolytic cleavages (e.g., proenzyme activation and intein excision), cross-linking reactions (e.g., disulfide bond formation and metal coordination), and side chain modifications (e.g., glycosylation and phosphorylation). Amino acid side chain modifications alone expand the protein code from 20 to 23 naturally encoded amino acids, to more than 350 modified amino acids (RESID Database of Protein Modifications,[2] http://www.ncifcrf.gov/RESID/). Proteins drive a subset of these PTMs to create novel cofactors, metal ligands, catalysts, and fluorophores by side chain covalent cross-linking, oxygen incorporation, carbamylation, methylation, oxidation, dehydration, and additional chemical reactions.[3] A particularly intriguing transformation is the spontaneous peptide backbone cyclization and oxidation chemistry required to convert three component amino acids into the fluorophore of the green fluorescent protein (GFP) family.

GFP and its homologs use an 11-stranded β-barrel protein architecture (Figure 1A) to drive fluorophore (Figure 2A) biosynthesis on a distorted central helix from the Ser65, Tyr66, and Gly67 tripeptide.[4,5] The resulting fluorophore (emission peak at 509 nm) exhibits absorbance maxima at 395 nm (protonated) and 475 nm (deprotonated), which are pH dependent and inversely correlated with the protonation state of nearby Glu222.[6,7] The spontaneous maturation[6] and tunable fluorescence properties of the fluorophores of GFP, its homologs,[8] and mutants[9,10] have revolutionized in vivo molecular tagging and

† Current address: Department of Chemistry, Texas A&M University, College Station, TX 77842.

(1) Harrison, P. M.; Kumar, A.; Lang, N.; Snyder, M.; Gerstein, M. *Nucleic Acids Res.* **2002**, *30*, 1083−1090.
(2) (a) Garavelli, J. S. *Proteomics* **2004**, *4*, 1527−1533. (b) Garavelli, J. S. *Nucleic Acids Res.* **2003**, *31*, 499−501.
(3) Okeley, N. M.; van der Donk, W. A. *Chem. Biol.* **2000**, *7*, R159−R171.
(4) Yang, F.; Moss, L. G.; Phillips, G. N., Jr. *Nat. Biotechnol.* **1996**, *14*, 1246−1251.
(5) Ormö, M.; Cubitt, A. B.; Kallio, K.; Gross, L. A.; Tsien, R. Y.; Remington, S. J. *Science* **1996**, *273*, 1392−1395.
(6) Tsien, R. Y. *Annu. Rev. Biochem.* **1998**, *67*, 509−544.
(7) Elsliger, M. A.; Wachter, R. M.; Hanson, G. T.; Kallio, K.; Remington, S. J. *Biochemistry* **1999**, *38*, 5296−5301.
(8) (a) Matz, M. V.; Fradkov, A. F.; Labas, Y. A.; Savitsky, A. P.; Zaraisky, A. G.; Markelov, M. L.; Lukyanov, S. A. *Nat. Biotechnol.* **1999**, *17*, 969−973. (b) Labas, Y. A.; Gurskaya, N. G.; Yanushevich, Y. G.; Fradkov, A. F.; Lukyanov, K. A.; Lukyanov, S. A.; Matz, M. V. *Proc. Natl. Acad. Sci. U.S.A.* **2002**, *99*, 4256−4261.
(9) Heim, R.; Prasher, D. C.; Tsien, R. Y. *Proc. Natl. Acad. Sci. U.S.A.* **1994**, *91*, 12501−12504.

10.1021/ja063983u CCC: $37.00

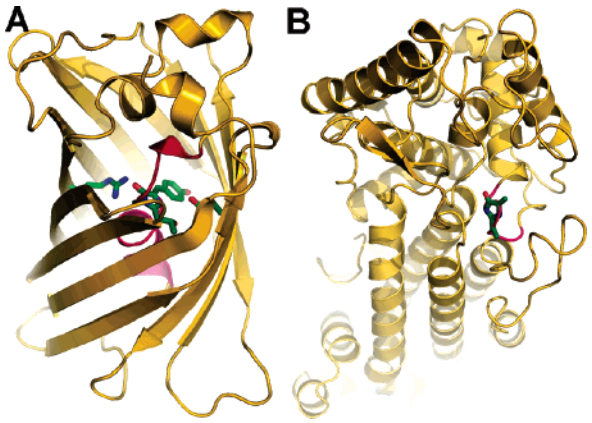

Figure 1. Overall topology and location of post-translational modification in GFP and HAL: (A) GFP overall β-barrel fold shown with buried chromophore (center), Arg96 (left), and Glu222 (right) in green, with oxygen atoms red, nitrogen atoms blue, and the central distorted helix in pink; (B) HAL overall α-helical fold shown with solvent-accessible MIO catalyst in green and loop in pink.

cell labeling. The significance of this PTM chemistry is furthermore underscored by the observation that the enzymes histidine ammonia lyase (HAL) (Figure 1B),[11] phenylalanine ammonia lyase (PAL),[12] and tyrosine aminomutase (TAM)[13] use a similar tripeptide backbone cyclization reaction to create their electrophilic methylidene-imidazole-5-one (MIO) catalysts[14] (Figure 2B). Both the GFP fluorophore and HAL/PAL/TAM MIO post-translational modifications entail three major biosynthetic steps: backbone cyclization via covalent bond formation between glycine nitrogen (Gly67 in GFP, Gly144 in HAL) and carbonyl carbon atoms (Ser65 in GFP, Ala142 in HAL), dehydration of the same carbonyl carbon, and either Tyr66 oxidation (GFP)[9,15,16] or Ser143 dehydration (HAL)[11,17] reactions to generate Cα−Cβ exocyclic double bonds and mature ring systems. Thus, despite dramatically different protein environments and architectures (Figure 1), these proteins undergo similar protein self-modification reactions to create five-membered imidazolone moieties (Figure 2). Understanding how protein architectures drive these amino acid transformations is critical to deciphering the chemical mechanisms for these key PTMs, to the informed design of self-modifying proteins with novel catalytic or reporter properties, and to a general understanding of how proteins control such complex PTM chemistries.

The GFP/RFP protein architectures conserve three elements (Figure 1A) to drive fluorophore biosynthesis: (1) a bend in the central chromophore-containing helix that removes inhibitory main chain hydrogen bonds and aligns molecular orbitals for ring formation,[18,19] (2) positively charged Arg96 to stabilize this helical bend and provide electrostatic interactions that are

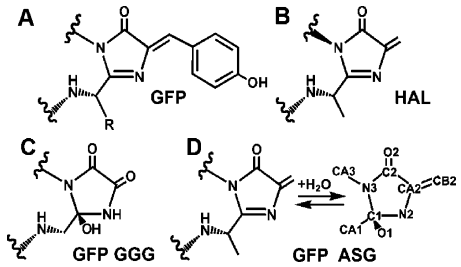

Figure 2. Molecular structures of imidazolone products after backbone cyclization and other post-translational modifications: (A) GFP chromophore (PDB 1EMA); (B) HAL MIO catalyst (PDB 1B8F); (C) cyclized ring for GFP GGG variant (PDB 1QYQ); (D) post-translational products for GFP ASG variants in aromatic/dehydrated (PDB 1YJF) and nonaromatic/hydroxylated (PDB 1YJ2) states.

important for ring formation,[18−21] and (3) negatively charged Glu222 to mediate Tyr66 Cα proton abstraction[20] and enolate intermediate formation.[22] Interestingly, in addition to chromophore biosynthesis, the GFP scaffold can promote other complex protein self-modification chemistry. Five relevant examples are of special interest for the work reported here: (1) an oxidative cross-link between the Y66L-substituted GFP chromophore and His148,[23] (2) chromophore-mediated decarboxylation of Glu222 upon intense light excitation,[24] (3) oxygen incorporation at the Y66G Cα position in the S65G Y66G variant, renamed GGG for the chromophore residues (Figure 2C),[18] (4) creation of dehydroalanine moieties through HAL-like dehydration rather than GFP-like oxidation chemistry for S65A Y66S (GFPhal or ASG) variants (Figure 2D),[19] and (5) spontaneous peptide hydrolysis and subsequent decarboxylation for S65G Y66S (GSG) variants.[25] In particular, we are interested in identifying and testing features that contribute to the remarkably diverse reactivity of this proteins scaffold.

Here we discovered additional unusual PTM chemistry with implications for the biosynthetic mechanism of the native chromophore. We present here four high-resolution structures indicating that Y66F variants partition between native Cα−Cβ oxidation and Cα−Cβ cleavage reaction pathways, depending on the protonation equilibrium for nearby Glu222. We further discovered a variant that, after Cα−Cβ cleavage, undergoes a Glu222-assisted oxygen incorporation reaction at the Y66F Cα atom. Together these data and analyses prompt the proposal of radical-based chemical mechanisms for Y66F Cα−Cβ cleavage, oxygen incorporation and fluorophore maturation, and support a common one-electron oxidized radical intermediate for chromophore biosynthesis in the GFP family.

Results

Crystallographic Structure and Analyses of the TFG Variant. To better understand the pH-dependent spectral properties of the GFP chromophore, we designed and constructed a GFP variant lacking the phenolic hydroxyl of the

(10) Heim, R.; Tsien, R. Y. *Curr. Biol.* **1996**, *6*, 178−182.
(11) Schwede, T. F.; Retey, J.; Schulz, G. E. *Biochemistry* **1999**, *38*, 5355−5361.
(12) Calabrese, J. C.; Jordan, D. B.; Boodhoo, A.; Sariaslani, S.; Vannelli, T. *Biochemistry* **2004**, *43*, 11403−11416.
(13) Christenson, S. D.; Liu, W.; Toney, M. D.; Shen, B. *J. Am. Chem. Soc.* **2003**, *125*, 6062−6063.
(14) Poppe, L. *Curr. Opin. Chem. Biol.* **2001**, *5*, 512−524.
(15) Cubitt, A. B.; Heim, R.; Adams, S. R.; Boyd, A. E.; Gross, L. A.; Tsien, R. Y. *Trends Biochem. Sci.* **1995**, *20*, 448−455.
(16) Reid, B. G.; Flynn, G. C. *Biochemistry* **1997**, *36*, 6786−6791.
(17) Baedeker, M.; Schulz, G. E. *Structure* **2002**, *10*, 61−67.
(18) Barondeau, D. P.; Putnam, C. D.; Kassmann, C. J.; Tainer, J. A.; Getzoff, E. D. *Proc. Natl. Acad. Sci. U.S.A.* **2003**, *100*, 12111−12116.
(19) Barondeau, D. P.; Kassmann, C. J.; Tainer, J. A.; Getzoff, E. D. *Biochemistry* **2005**, *44*, 1960−1970.
(20) Sniegowski, J. A.; Lappe, J. W.; Patel, H. N.; Huffman, H. A.; Wachter, R. M. *J. Biol. Chem.* **2005**, *280*, 26248−26255.
(21) Wood, T. I.; Barondeau, D. P.; Hitomi, C.; Kassmann, C. J.; Tainer, J. A.; Getzoff, E. D. *Biochemistry* **2005**, *44*, 16211−16220.
(22) Barondeau, D. P.; Tainer, J. A.; Getzoff, E. D. *J. Am. Chem. Soc.* **2006**, *128*, 3166−3168.
(23) Rosenow, M. A.; Patel, H. N.; Wachter, R. M. *Biochemistry* **2005**, *44*, 8303−8311.
(24) (a) Bell, A. F.; Stoner-Ma, D.; Wachter, R. M.; Tonge, P. J. *J. Am. Chem. Soc.* **2003**, *125*, 6919−6926. (b) van Thor, J. J.; Gensch, T.; Hellingwerf, K. J.; Johnson, L. N. *Nat. Struct. Biol.* **2002**, *9*, 37−41.
(25) Barondeau, D. P.; Kassmann, C. J.; Tainer, J. A.; Getzoff, E. D. *J. Am. Chem. Soc.* **2006**, *128*, 4685−4693.

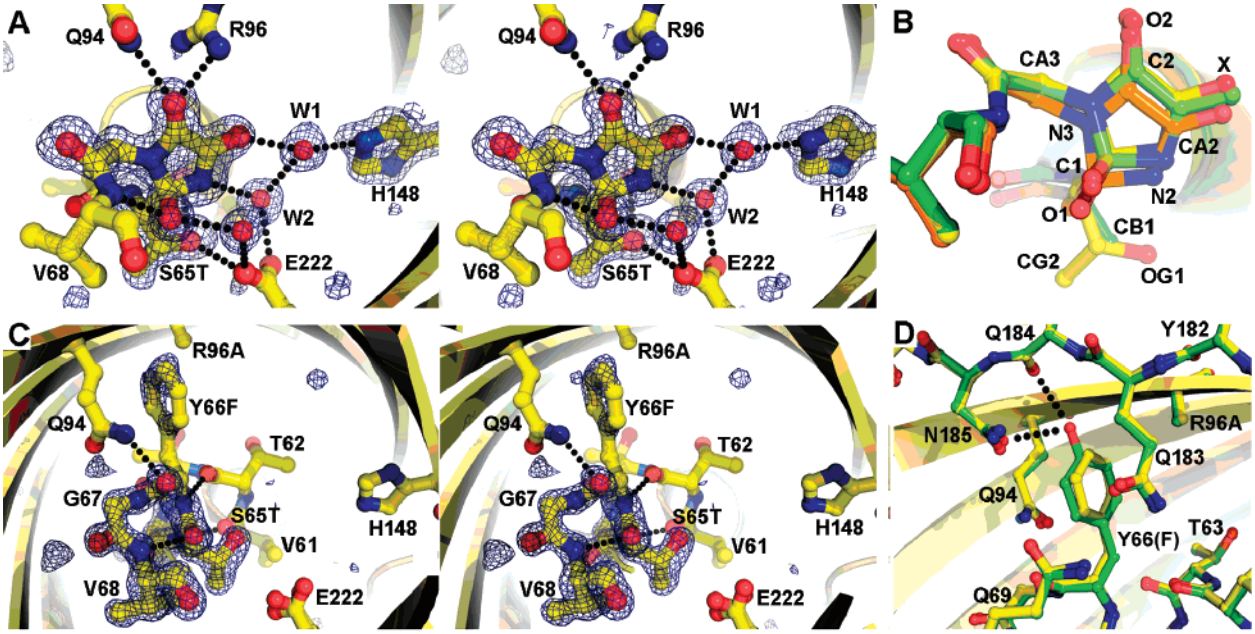

Figure 3. Crystallographic structures of TFG and TFG R96A variants. (A) Stereo pair for the TFG variant (yellow, with red oxygen and blue nitrogen atoms) displayed with $F_o - F_c$ omit (chromophore and His148 omitted) electron density map contoured at 3σ (dark blue) at 1.35 Å resolution. The Cα backbone ribbon is shown in yellow, hydrogen bonds as black dotted lines, and water molecules (also omitted) as red spheres. (B) Structural overlay of TFG (yellow), ASG (green, PDB code 1YJ2), and GGG (orange, 1QYQ) with atom labels. The exocyclic atom is labeled as X. (C) Stereo pair for the TFG R96A variant (yellow) displayed with $F_o - F_c$ omit (residue 65−67 omitted) electron density map contoured at 4σ (dark blue) at 1.20 Å resolution E222 exhibits two conformations. (D) Overlay of precursor TFG R96A (yellow) and R96A (green, PDB code 1QY3) structures. Hydrogen bonds from the Y66 side chain hydroxyl are shown as black dotted lines.

Table 1. Diffraction Data Collection and Refinement Statistics

	TFG	TFG R96A	AFG	AFG E222A
resolution (Å)	40.0−1.35	20.0−1.20	20.0−1.60	20.0−2.05
last shell (Å)[a]	1.40−1.35	1.24−1.20	1.66−1.60	2.12−2.05
unit cell (Å)	51.2 62.5 71.2	51.4 62.8 70.5	51.0 62.4 71.1	51.4 62.4 68.7
observations	195055	188735	105935	67620
unique observations	50300	61453	29628	13519
R_{sym} (%)[b]	4.3 (35.2)	3.0 (29.7)	5.1 (26.2)	7.0 (35.7)
completeness (%)	98.9 (97.2)	85.6 (34.2)	96.0 (77.9)	93.1 (85.2)
$\|/\sigma\|$	26.2 (3.1)	32.5 (2.2)	20.6 (2.7)	20.2 (4.8)
refined parameters	19371	19820	8136	7536
R_{work}/R_{free} (%)[c]	14.5/20.2	15.6/20.6	21.6/24.4	22.1/26.5
PDB code	2HCG	2HFC	2HGD	2HGY

[a] Values in parentheses are the statistics for the highest resolution shell of data. [b] $R_{sym} = \sum|I_{hkl} - \langle I\rangle|/\sum\langle I\rangle$, where $\langle I\rangle$ is the average individual measurement of I_{hkl}. [c] $R_{work} = (\sum|F_{obs} - F_{calc}|) / \sum|F_{obs}|$ where F_{obs} and F_{calc} are the observed and calculated structure factors, respectively. R_{free} is calculated the same as R_{work} but from the data (5%) that were excluded from the refinement.

tripeptide fluorophore (Y66F GFPsol, for details see Methods). Surprisingly, this TFG variant (renamed for chromophore residues) is essentially colorless, indicating that the chromophore did not form or that the resulting cyclized ring lacked the extended conjugation required to exhibit a visible absorbance. In contrast, Cubitt et al. reported that another Y66F GFP variant, containing the SFG chromophore, exhibited an absorbance maximum at 360 nm and fluorescence emission at 442 nm.[15]

To understand the molecular basis for the colorless GFP TFG variant, we crystallized and determined its 1.35 Å resolution structure (Table 1). Omit and difference electron density maps revealed that the TFG sequence is cyclized, but remarkably, the side chain ring of Y66F is gone. This ring loss created a cavity that is filled by two water molecules (W1 and W2) and a rearranged side chain of His148 (Figure 3A), all of which would interpenetrate a GFP-like Y66F chromophore. The S65T carbonyl oxygen (O1) atom (see Figure 2D for atom labels) is still present (Figure 3A), as in some other modified chromophore variants,[18,19,26] whereas O1 is lost via main chain dehydration in the mature wild-type GFP chromophore.[4,5] In the TFG variant, the presence of the O1 hydroxyl makes the chromophore nonaromatic and explains the lack of visible absorbance. This O1 hydroxyl forms hydrogen bonds to a third water molecule and to the backbone amide of Val68 (Figure 3A). Furthermore, a single exocyclic non-hydrogen atom is attached to the Y66F Cα atom and in hydrogen-bonding distance from a water molecule (W1). This TFG post-translational product resembles those previously characterized for the GGG[18] and ASG[19] variants (Figure 2); all are nonaromatic ring systems that contain O1 hydroxyl groups and exocyclic non-hydrogen atoms located at the position of the wild-type Y66 Cβ atom (Figure 3B). Thus, the TFG self-modification could result from Cβ−Cγ bond cleavage, leaving an exocyclic carbon atom (ASG-like product; Figure 2D), or Cα−Cβ bond cleavage with subsequent oxygen

(26) Rosenow, M. A.; Huffman, H. A.; Phail, M. E.; Wachter, R. M. *Biochemistry* **2004**, *43*, 4464−4472.

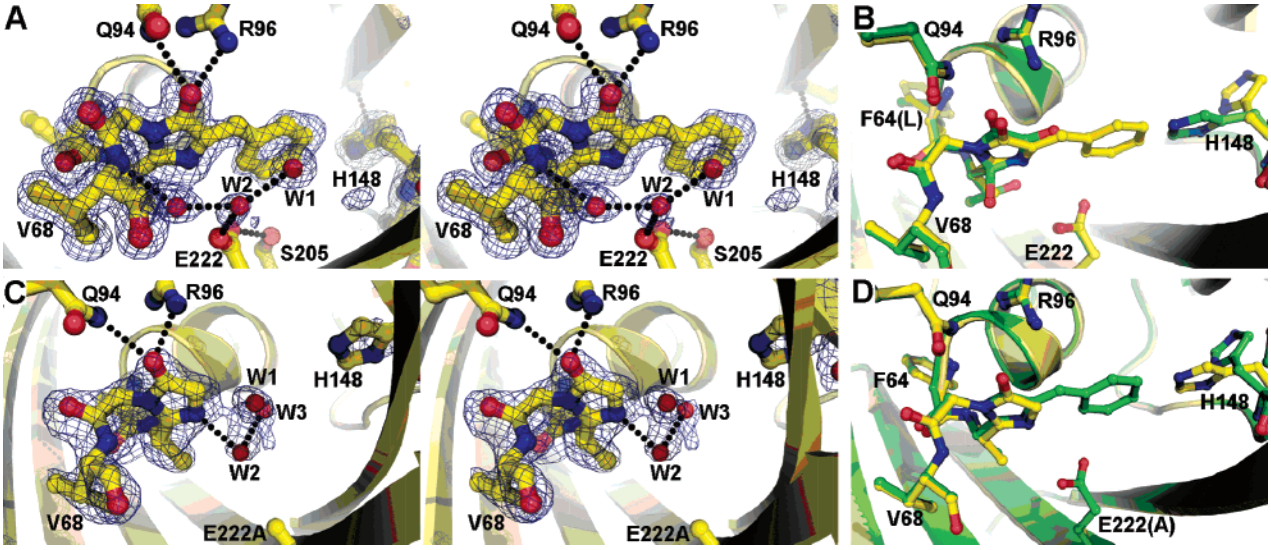

Figure 4. Crystallographic structures of AFG and AFG E222A variants. (A) Stereo pair for the AFG variant (yellow, with red oxygen and blue nitrogen atoms) displayed with $F_o - F_c$ omit (chromophore and His148 omitted) electron density map contoured at 3σ (dark blue) at 1.60 Å resolution. The Cα backbone ribbon is shown in yellow, hydrogen bonds as black dotted lines, and water molecules (also omitted) as red spheres. (B) Structural overlay of AFG (yellow) and TFG (green), highlighting the different conformations of His148 (right). (C) Stereo pair for the AFG E222A variant (yellow) displayed with $F_o - F_c$ omit electron density map contoured at 3.5σ (dark blue) at 2.05 Å resolution. (D) Overlay of AFG (green) and AFG E222A (yellow) structures highlighting Y66F side chain elimination coupled with E222A truncation and the different conformations of His148 (right).

incorporation to create an exocyclic oxygen atom (like the GGG variant; Figure 2C). Although our crystallographic data cannot readily discriminate between these two cleavage possibilities, the TFG structure unambiguously indicates an unusual PTM including carbon−carbon bond scission and ring elimination.

Structure of the TFG R96A Variant. Characterizing intermediates in the TFG post-translational chemistry is difficult, because cleavage and loss of the ring moiety occurs within the first few hours after recombinant protein induction. To help distinguish the position of the bond cleavage and identify the elimination product, we therefore constructed and characterized the more slowly maturing Y66F R96A GFPsol (TFG R96A) variant. Previously, we had established that the R96A substitution dramatically slows chromophore biosynthesis from hours to months and that maturation can occur within the protein crystal.[18] Here we introduced the R96A mutation into the TFG construct to slow chromophore maturation and potentially trap the Y66F elimination product inside the crystal lattice.

The TFG R96A structure was determined at 1.20 Å resolution (Table 1) and revealed a precyclized conformation for the chromophore residues (Figure 3C). The Y66F ring conformation in the TFG R96A structure is very similar to that previously observed for Tyr66 in the structure of a precyclized R96A variant[18] (Figure 3D). The Y66F side chain occupies a position near the R96A substitution and stacks between Gln94 and Gln183. Comparison of the Tyr66 and Y66F side chain positions indicated a slight difference in ring tilt likely due to the loss of hydrogen bonds from the Tyr66 phenolic oxygen to the Asn185 side chain and carbonyl oxygen of Gln184.

Interestingly, the omit $F_o - F_c$ difference maps for TFG R96A exhibited strong electron density for the Y66F ring and the backbone carbonyl and nitrogen atoms, but weak electron density connecting the Y66F Cα and Cβ atoms (Figure 3C). We hypothesized that this weak electron density was due to a minor population of Cα−Cβ cleaved product. To test if this variant was slowly undergoing the cleavage reaction inside the crystal lattice, we collected and analyzed additional TFG R96A data sets after prolonged crystal incubation times (>2 years). The resulting electron density maps (not shown) appeared the same, with the Y66F ring intact but weak electron density between the Cα and Cβ atoms. Thus, cleavage is not ongoing in TFG R96A crystals.

The presence of the intact Y66F benzyl group in TFG R96A indicated that either the TFG elimination reaction follows imidazolone ring formation and/or the positively charged Arg96 accelerates the elimination reaction. Since our strategy to trap the cleavage product inside the crystal lattice was unsuccessful, we constructed the Y66F ASG variant (renamed AFG for the chromophore residues; see Methods) to test if Y66F variants, like Y66S variants, undergo a GFPhal-like[19] post-translational elimination reaction by cleaving the Cβ−Cγ bond. Such a cleavage reaction in Y66F GFP variants would also resemble the elimination of the substrate adduct during the PAL catalytic cycle[27] (see Figure 5C, reaction 3). Furthermore, we reasoned that if the Y66F elimination reaction proceeds through Cβ−Cγ cleavage, similar to Cβ−Oγ cleavage in Y66S variants, then the resulting PTMs of AFG and ASG,[20] which are identical except for the Y66F versus Y66S substitution, should exhibit the same spectroscopic and structural properties.

Spectroscopic and Structural Characterization of the AFG Variant. The AFG variant exhibited an absorbance maximum at 347 nm that is blue-shifted from both the SFG (360 nm)[15] and ASG (385 nm)[19] chromophores. Thus, we anticipated that the AFG chromophore was a cyclized, dehydrated moiety that was less conjugated (likely cleaved) than the SFG and ASG chromophores. Surprisingly, the 1.60 Å resolution structure of the AFG variant (Table 1) revealed a cyclized, dehydrated GFP-like (*more conjugated*) chromophore that retained its Y66F side chain (Figure 4A). The AFG and TFG variants therefore undergo different post-translational chemistry: GFP-like oxidation for AFG compared to carbon−carbon cleavage for TFG. Outside of the chromophore residues, the only significant differences

(27) Langer, B.; Langer, M.; Retey, J. *Adv. Protein Chem.* **2001**, *58*, 175−214.

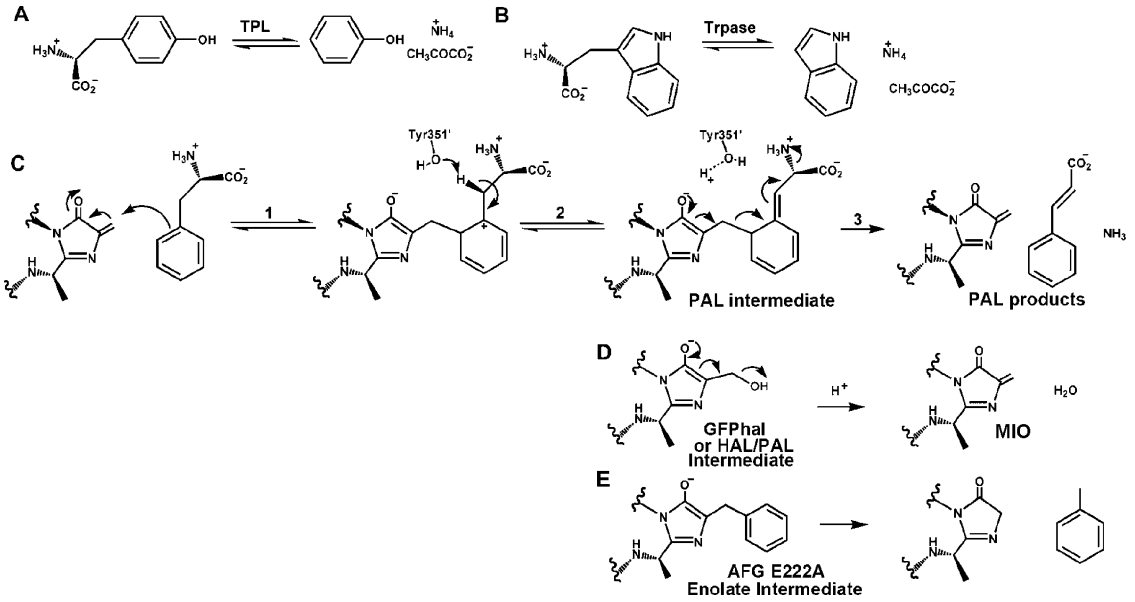

Figure 5. Comparison of enzymatic and post-translational carbon−carbon bond cleavage and elimination reactions. (A) Carbon−carbon bond cleavage reaction catalyzed by tyrosine phenol-lyase (TPL). (B) Carbon−carbon bond cleavage reaction catalyzed by tryptophan indole-lyase (Trpase). (C) Reaction scheme for phenylalanine ammonia lyase (PAL): (1) adduct formation between Phe and the MIO catalyst, (2) deprotonation and Cβ−Cγ double-bond formation, and (3) adduct degradation and loss of ammonia. (D) MIO biosynthesis in HAL/PAL and GFPhal. (E) Cα−Cβ bond cleavage reaction for the AFG E222A variant.

between these structures are the conformation of His148 (Figure 4B), which rearranged (compared to wild-type GFP) in TFG to fill the cavity left by the Y66F side chain cleavage, and the implied protonation state of Glu222. In TFG, the S65T side chain hydroxyl simultaneously formed hydrogen bonds to both Glu222 (Figure 3A) and the backbone oxygen atom of Val61, thereby implicating a protonated Glu222 carboxylic acid as a hydrogen bond donor. In AFG, the S65A side chain cannot participate in a hydrogen bond with Glu222, and Glu222 is likely deprotonated. This correlation between the side chain of residue 65 and the protonation state of Glu222 has been previously characterized for Tyr66 GFP variants.[6,7] Thus, we postulate that the protonation equilibrium of Glu222 controls the post-translational outcome for Y66F variants; the S65T substitution and predominantly neutral Glu222 of the TFG variant result in the unusual elimination reaction, whereas the S65A substitution and predominantly negatively charged Glu222 of the AFG variant favor a GFP-like oxidation reaction pathway.

Structure and Characterization of the AFG E222A Variant. To test this hypothesis, we designed the AFG E222A variant (see Methods), which lacks the Glu222 negative charge and is therefore predicted to undergo ring elimination. The AFG E222A variant exhibited a 362 nm absorbance maximum that is distinct from AFG (347 nm) and very similar to the SFG variant (360 nm).[15] Omit difference electron density maps for the 2.05 Å resolution AFG E222A structure (Table 1) indicated formation of a cyclized imidazolone ring moiety that lacked the Y66F benzyl group (Figure 4C). Unlike the post-translational product for TFG, dehydration has occurred for AFG E222A: the five-membered imidazolone ring lacks the O1 hydroxyl group and is therefore planar (and aromatic), explaining its visible absorbance properties. Truncation of Glu222 via the E222A mutation resulted in minor Cβ−Cγ rotations for the nearby hydrophobic residues Leu42, Leu44, and Leu220. In addition, diffuse electron density that was modeled as three water molecules filled the resultant cavity (Figure 4C). The ring plane for this AFG E222A imidazolone moiety is tilted ~9° compared to that in the AFG structure (Figure 4D). Intriguingly, there is no exocyclic atom attached at the Y66F Cβ position of the AFG E222A PTM. Thus, the AFG E222A PTM product provides insights into two roles of Glu222 in GFP PTMs: the cleavage position for Y66F variants and the cleavage versus oxidation partitioning mechanism (see Discussion). Together our results (Table 2) indicate that the unusual Y66F elimination pathway requires ring formation and/or positively charged Arg96, whereas negatively charged Glu222 favors an oxidative GFP-like PTM pathway.

Table 2. Post-Translational Outcome for Y66F Variants

variant	E222[a]	R96	cyclization	elimination	dehydration	oxidation[b]
AFG	negative	positive	yes	no	yes	yes
TFG	neutral	positive	yes	yes	no	yes
AFG E222A	absent	positive	yes	yes	yes	no
TFG R96A	neutral	absent	no	no	no	no

[a] Favored protonation state of Glu222. [b] Oxidation is either Cα−Cβ double-bond formation (AFG) or Cα oxygen incorporation (TFG).

Discussion

Spectroscopic Properties. The spectroscopic properties of the Y66F and Y66S GFP variants are difficult to rationalize based solely on chromophore conjugation. Crystallographic structures reveal that the cyclized chromophores for the AFG, ASG, and AFG E222A variants differ in the substituents bound at the residue 66 Cα atoms: a benzyl group for AFG, a vinyl group for ASG, and a hydrogen atom for AFG E222A. However, the absorbance maxima follow the series ASG (385 nm; vinyl)[19] > AFG E222A (362 nm; hydrogen) > AFG (347 nm; benzyl). Comparison of the AFG and AFG E222A structures (Figure 4D) indicates a tilt of the imidazolone ring plane by ~9°, which could represent ground state destabilization for the AFG variant and result in its blue-shifted absorbance properties. The spectroscopic properties may also be influenced

by the protonation state of the imidazolone N2 nitrogen (see Figure 2D) and thus indirectly by the protonation state of Glu222; the distance between the N2 atom and the nearest carboxylate oxygen atom of Glu222 is ~3.7 Å in the AFG variant. It is also interesting that the SFG variant[15] exhibits absorbance properties (360 nm) most similar to those of the AFG E222A variant (362 nm), which has undergone carbon−carbon cleavage rather than oxidation chemistry. Nevertheless, the most fascinating aspect of the Y66F variants is not their spectroscopic properties but the unusual carbon−carbon bond cleavage and elimination of unactivated carbon leaving groups.

Carbon−Carbon Bond Cleavage for Aromatic Amino Acids. Some Y66F GFP variants undergo surprising cleavage of carbon−carbon bonds, which normally have bond energies of ~350 kJ/mol. The enzymes tyrosine phenol-lyase (TPL) and tryptophan indole-lyase (Trpase) utilize a pyridoxal-5′-phosphate (PLP) cofactor to catalyze similar carbon−carbon (Cβ−Cγ) bond cleavage reactions for their L-tyrosine (Figure 5A) and L-tryptophan (Figure 5B) substrates, respectively.[28] Phenylalanine and histidine ammonia lyase (PAL and HAL),[12,14,27] on the other hand, utilize a GFP-like MIO electrophile to catalyze substrate adduct formation, carbon−carbon bond cleavage, and product formation (Figure 5C). These enzymes all use electrophiles (either cofactors or post-translational products) to degrade aromatic amino acids. Interestingly, the proposed enolate intermediate[22] for the Y66F GFP variants (Figure 5E) contains an electrophilic imidazolone ring resembling intermediates in the PAL catalytic cycle (Figure 5C) and biosynthesis of HAL/PAL post-translational modifications (Figure 5D). There is also precedent for HAL-like elimination chemistry in the GFP scaffold; the ASG variants change the post-translational chemistry from GFP-like oxidation to HAL-like dehydration.[19] Despite these apparent similarities, the Y66F cleavage position and elimination chemistry are distinct.

Our AFG E222A structure indicated Cα−Cβ cleavage in Y66F, unlike the cleavage of Cβ−Cγ in TPL and Trpase, Cβ−hydroxyl in MIO biosynthesis, and Cβ−adduct during PAL/HAL catalysis (Figure 5). Neither the AFG E222A nor the TFG crystal structure has electron density for the Y66F side chain ring (Figure 4C, 3A), and both exhibit significant rearrangements of the His148 ring (compared to wild-type and AFG GFP; Figure 4B,D) to a position that would interpenetrate the Y66F side chain ring in an uncleaved GFP-like chromophore, like that of AFG (Figure 4A). Because these structures were determined at cryogenic temperature, both the lack of a trapped elimination product and the His148 ring position are incompatible with an uncleaved chromophore. Thus, the Cα−Cβ cleavage does not appear to be induced as radiation damage during X-ray diffraction data collection, but, more likely, from prior spontaneous post-translational self-modification reactions. Searching the RESID post-translational modification database[2] revealed no other examples for spontaneous phenylalanine Cα−Cβ cleavage in proteins. Therefore, the Y66F elimination products are generated through an unprecedented post-translational carbon−carbon bond cleavage mechanism with loss of poor leaving group (a benzyl moiety).

Scheme 1. Reaction Scheme for Y66F Carbon−Carbon Bond Cleavage[a]

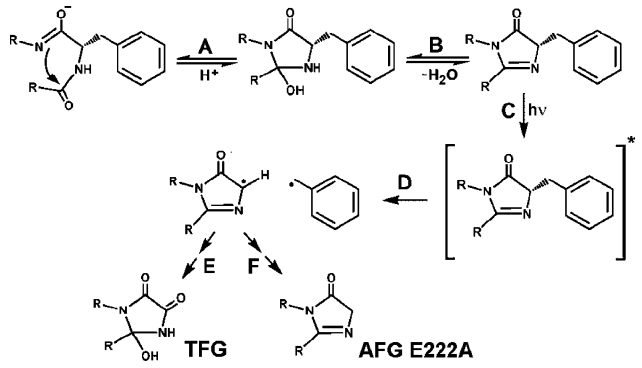

[a] (A) Backbone cyclization; (B) main chain dehydration; (C) photoexcitation of dehydrated intermediate; (D) homolytic Cα−Cβ bond cleavage; (E) hydration and oxidation to form TFG PTM product (see Scheme 2); (F) hydrogen atom transfer to generate the AFG E222A PTM product.

Despite this novelty for Cα−Cβ cleavage of phenylalanine in proteins, there are precedents for radical-based cleavage of Phe-containing peptides, through photochemical and X-ray-induced reactions. Fasanella and Gordy established that irradiation of phenylalanine generates carbon−carbon bond cleavage and a long-lived benzyl radical,[29] whereas irradiation of tyrosine results in loss of H from the hydroxyl group attached to the ring.[30] Hayon and co-workers used flash photolysis studies to establish that Phe generates benzyl radicals and hydrated electrons through photodissociative and photoionization processes, respectively.[31,32] Moreover, in a comparative study of X-ray-induced decomposition of Phe and Tyr, Zubavichus et al. identified multiple Phe products, including species that had undergone Cα−Cβ bond cleavage, whereas the carbon skeleton of Tyr remained intact.[33] Together these publications show substantial evidence for Cα−Cβ cleavage of phenylalanine (but not tyrosine). This cleavage is radical-based, appears to be independent of the radiation source (method) for radical generation, and exhibits chemistry analogous to the spontaneous post-translational modifications described herein for Y66F GFP variants. The common theme of radical chemistry for Cα−Cβ cleavage reactions in phenylalanine-containing amino acids and peptides hints at similar radical-based mechanisms for Y66F degradation in GFP variants.

Mechanism of Spontaneous Y66F Elimination. We propose a shared homolytic radical scission mechanism (Scheme 1) for the spontaneous Cα−Cβ cleavage reactions of GFP Y66F variants TFG and AFG E222A. In this mechanism, backbone cyclization (Scheme 1A) and main chain dehydration (Scheme 1B) precede cleavage and produce the dehydrated intermediate, following the mechanism proposed for wild-type GFP.[15] Next, photoexcitation of the dehydrated intermediate (Scheme 1C)

(28) (a) Phillips, R. S.; Demidkina, T. V.; Faleev, N. G. *Biochim. Biophys. Acta* **2003**, *1647*, 167−172. (b) Lee, M.; Phillips, R. S. *Bioorg. Med. Chem.* **1995**, *3*, 195−205. (c) Phillips, R. S.; Bender, S. L.; Brzovic, P.; Dunn, M. F. *Biochemistry* **1990**, *29*, 8608−8614. (d) Demidkina, T. V.; Zakomirdina, L. N.; Kulikova, V. V.; Dementieva, I. S.; Faleev, N. G.; Ronda, L.; Mozzarelli, A.; Gollnick, P. D.; Phillips, R. S. *Biochemistry* **2003**, *42*, 11161−11169.

(29) Fasanella, E. L.; Gordy, W. *Proc. Natl. Acad. Sci. U.S.A.* **1969**, *64*, 1−7.
(30) Fasanella, E. L.; Gordy, W. *Proc. Natl. Acad. Sci. U.S.A.* **1969**, *62*, 299−304.
(31) Bent, D. V.; Hayon, E. *J. Am. Chem. Soc.* **1975**, *97*, 2606−2612.
(32) (a) Mittal, L. J.; Mittal, J. P.; Hayon, E. *J. Am. Chem. Soc.* **1973**, *95*, 6203−6210. (b) Mittal, L. J.; Mittal, J. P.; Hayon, E. *Chem. Phys. Lett.* **1973**, *18*, 319−322.
(33) Zubavichus, Y.; Zharnikov, M.; Shaporenko, A.; Fuchs, O.; Weinhardt, L.; Heske, C.; Umbach, E.; Denlinger, J. D.; Grunze, M. *J. Phys. Chem. A* **2004**, *108*, 4557−4565.

Scheme 2. Reaction Scheme for Oxygen Incorporation Reaction in TFG[a]

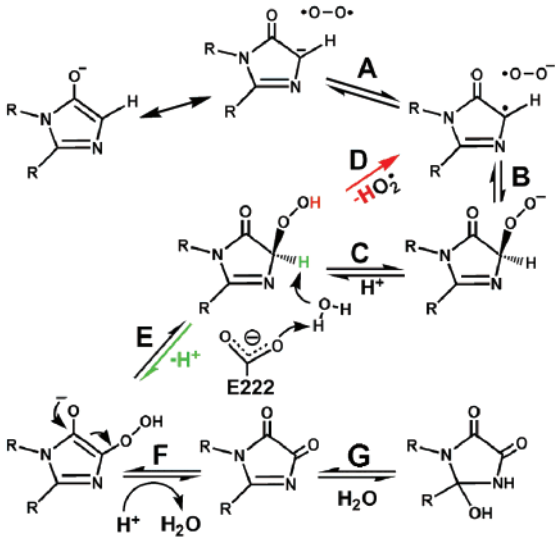

[a] (A) Electron transfer to generate superoxide and a chromophore radical; (B) radical recombination to make a peroxy adduct; (C) protonation to generate a hydroperoxy intermediate; (D) loss of the hydroperoxy moiety and regeneration of the resonance-stabilized chromophore radical; (E) Glu222-mediated deprotonation of the Cα atom; (F) loss of water and generation of a dicarbonyl moiety; (G) hydration to form the observed TFG crystallographic product.

leads to homolytic radical cleavage (Scheme 1D), creating two resonance-stabilized carbon-based radical products: a benzyl radical and an aromatic ring moiety that contains a secondary radical at the Y66F Cα position. This ring moiety can then go on to form the TFG (Schemes 1E and 2) and AFG E222A (Scheme 1F) products, whereas the benzyl elimination product can diffuse out of the GFP β-barrel. This mechanism has precedent in the photochemical radical-based cleavage of Phe-containing peptides.[31] In fact, Bent and Hayon[31] conclude that "contrary to earlier views, direct optical excitation of Phe in proteins may be expected to lead to some dissociation reactions". Notably, the susceptibility of Phe, but not Tyr, peptides to radical-induced Cα−Cβ cleavage explains the carbon−carbon cleavage of Y66F, but not Tyr66, GFP variants. Furthermore, light-dependent radical mechanisms also have been proposed in GFP for PTM decarboxylation reactions of E222[24] and the S65T carboxyl terminus (after a spontaneous peptide hydrolysis reaction).[25]

Oxygen Incorporation Reaction. We also propose a related radical-based mechanism (Scheme 2) for oxygen incorporation in the TFG variant (Scheme 1E) after homolytic cleavage of the Y66F Cα−Cβ bond (Scheme 1D). In this mechanism, the radical aromatic ring cleavage product combines with superoxide to form a peroxy adduct (Scheme 2B). Next, protonation produces a hydroperoxy intermediate (Scheme 2C), which partitions into two distinct post-translational outcomes, influenced by the presence or absence of negatively charged Glu222. When present, Glu222 facilitates water-mediated Cα deprotonation (Scheme 2E) in variants such as GGG[18] and TFG. The role of conserved Glu222 as a base is consistent with a previous proposal in GFP chromophore maturation.[20] After Cα proton abstraction, mediated by Glu222, subsequent loss of water (Scheme 2F) generates a dicarbonyl species that can be hydrated at the S65T C1 atom (Scheme 2G) to form the observed TFG

Scheme 3. Reaction Mechanism for AFG (and Native) GFP Chromophore Biosynthesis, Highlighting Partitioning between Cα−Cβ Oxidation and Cleavage Reactions in AFG GFP[a]

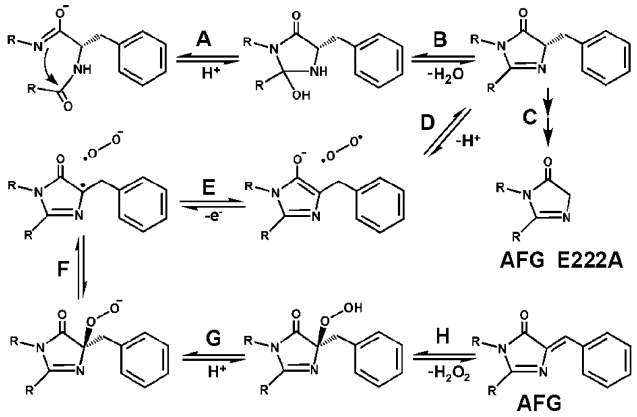

[a] (A) Backbone cyclization; (B) main chain dehydration; (C) homolytic bond cleavage to produce the observed FG E222A crystallographic product (see Scheme 1); (D) deprotonation and enolate intermediate formation; (E) electron transfer to generate superoxide and a chromophore radical; (F) radical recombination to form a peroxy adduct; (G) protonation to generate a hydroperoxy adduct; (H) loss of hydrogen peroxide to generate the observed AFG crystallographic product (and mature native GFP chromophore).

crystallographic product. This oxygen incorporation reaction[15,18,19,22] for GGG and for TFG (after cleavage) is likely directly relevant to the rate-limiting Cα−Cβ oxidation reaction for GFP chromophore maturation.

GFP variants lacking Glu222, such as AFG E222A, fail to mediate Cα proton abstraction (Scheme 2E) during the lifetime of the hydroperoxy intermediate. Instead, this intermediate undergoes radical cleavage (Scheme 2D) releasing a hydroperoxy moiety and regenerating the same resonance-stabilized aromatic radical moiety formed during Cα−Cβ cleavage of Y66F variants (Scheme 1D). This produces a futile cycle of oxygen incorporation and loss (Scheme 2B−D). In addition, this radical cleavage product can undergo one-electron reduction to regenerate the enolate intermediate (Scheme 2A). Our data therefore indicates that Glu222 controls the branchpoint partition between oxidation via Cα deprotonation and a futile cycle of oxygen incorporation and hydroperoxide loss.

Chromophore Biosynthesis. We propose a mechanism for Y66F (and native) GFP chromophore biosynthesis (Scheme 3) with many similarities to oxygen incorporation (Scheme 2), including a one-electron oxidized radical intermediate. In this biosynthetic scheme, cyclization (Scheme 3A) and dehydration (Scheme 3B) precede oxidation, consistent with previous proposals.[15,18,19,22] The dehydrated intermediate then partitions between Cα−Cβ cleavage (Scheme 3C) and Cα deprotonation coupled to enolate formation (Scheme 3D). The resultant aromatic enolate intermediate[22] is resonance stabilized by six π-electrons: two for the lone pair on the Gly67 nitrogen, plus one each for the other four members of the imidazolone ring system. A one-electron oxidation of the enolate intermediate (Scheme 3E) creates a carbon-based radical species like that generated in Scheme 2A. This reaction has precedent in the radiolysis-induced oxidation of amino acids,[34] which proceeds through an initial Cα hydrogen atom abstraction step. Because the dehydrated enolate resonance stabilizes both the

(34) Stadtman, E. R. *Annu. Rev. Biochem.* **1993**, *62*, 797−821.

cleavage product (Scheme 3C) and the one-electron oxidized intermediate (Scheme 3E), we favor this cyclization−dehydration−oxidation mechanism (Scheme 3), over the alternative cyclization−oxidation−dehydration model.[26,35]

We hypothesize that molecular oxygen is the oxidant necessary to generate the radical intermediate for GFP chromophore biosynthesis (Scheme 3E). We previously suggested that molecular oxygen binds near conserved Arg96, which provides positive electrostatic interactions that may facilitate electron transfer from the chromophore to oxygen for superoxide generation (Scheme 3E).[22] This proposed role for electrostatics in oxygen binding and chromophore oxidation has precedent in an analogous electron-transfer reaction for amine oxidase cofactor biogenesis.[36] In amine oxidase, positive electrostatic interactions from a copper ion facilitate one-electron cofactor (tyrosine) oxidation to produce superoxide and a radical cation.[36,37] Cu,Zn superoxide dismutase also provides positive electrostatic interactions for binding and electron transfer with oxygen/superoxide; superoxide binding to Arg and Cu promotes oxidation of superoxide to dioxygen or reduction to peroxide based upon the Cu oxidation state and active-site geometry.[38] Thus, there are precedents for protein systems that use electrostatics to drive one-electron chemistry, albeit through metal-assisted processes.

In GFP fluorophore biosynthesis, we propose recombination of this superoxide radical anion with the chromophore radical to generate a peroxy intermediate (Scheme 3F). Incorporating oxygen at the Cα position of residue 66 has precedent in the GGG[18] and TFG (Figure 3A) GFP variants. Next, we suggest protonation of the peroxy intermediate (Scheme 3G) and loss of hydrogen peroxide (Scheme 3H) to form a mature chromophore. This proposal is very analogous to that for amine oxidase in which a similar radical recombination reaction generates a peroxy intermediate, which is followed by further oxidation, hydrogen peroxide formation, and mature TPQ cofactor biogenesis.[36,37] Moreover, recent studies by the Wachter group show the generation of hydrogen peroxide is co-incident with chromophore formation, supporting a role for molecular oxygen in amino acid oxidation.[35] Coupled with previous results on GFP variants and related post-translational modifications, our Y66F data and analyses support a role for the GFP protein environment in promoting radical chemistry to activate molecular oxygen for controlled amino acid modifications.

Partitioning Role of Glu222. The S65T substitution, which favors neutral Glu222, increases the overall chromophore maturation rate for wild-type GFP (lowers the time constant from 2.0 to 0.45 h),[39] suggesting that the rate-limiting oxidation reaction has been accelerated. However, this substitution also switches the Y66F variants from GFP-like oxidative to carbon−carbon cleavage pathways. This apparent paradox can be explained if the mutation affects distinct rate-limiting and partitioning steps, and partitioning precedes the rate-limiting reaction. We suggest that the rate-limiting step for GFP fluorophore biosynthesis is oxidation of the enolate intermediate by molecular oxygen to form a radical moiety (Scheme 3E). In contrast, we postulate that the oxidation-cleavage partitioning step or branchpoint for Y66F variant is at the preceding dehydrated intermediate. As shown by our results (Table 2), the presence of negatively charged Glu222 favors Cα deprotonation and enolate formation (Scheme 3D) leading to chromophore oxidation, whereas the lack of this base allows homolytic cleavage (Scheme 3C). Glu222 also appears to have a similar partitioning role in the subsequent oxygen incorporation reaction; negatively charged Glu222 favors oxygen incorporation (Scheme 2E), whereas its absence leads to a futile cycle of oxygen incorporation and loss (Scheme 2B−D). A key difference between the two oxidation-cleavage partitioning step is that the Cα−Cβ cleavage reaction for Y66F variants is irreversible (Scheme 3C), whereas the loss of a hydroperoxy radical (Scheme 2D) regenerates the aromatic radical, which can undergo another cycle of oxygen incorporation (Scheme 2B).

Interestingly, Glu222 mutants do not change the post-translational product for wild-type GFP.[6,20] This can be explained by differences in the partitioning steps between wild-type Tyr66 GFP and Y66F GFP variants. As discussed above, Tyr66 does not promote Cα−Cβ bond cleavage, whereas Y66F does. Wild-type Cα−Cβ bond oxidation does not involve a second Glu-mediated Cα proton abstraction like that for TFG oxygen incorporation (Scheme 1). Variants that lack a Cβ atom for the central chromophore tripeptide residue, like GGG[39] and TFG (after Cα−Cβ cleavage), appear to undergo a second Glu-mediated Cα deprotonation, oxidation, and loss of water (Scheme 2). To explain the apparent dependence of the rate-limiting oxidation reaction on the protonation equilibrium for Glu222,[25,40] we suggest Glu222 also influences reaction steps after enolate formation (Scheme 3D). Together these results and analyses make a compelling case for both the one-electron oxidized intermediate and the radical-based mechanism for chromophore biosynthesis in this family of fluorescent proteins.

Post-Translational Modification Chemistry. Here we expand on the spontaneous self-modification chemistry available in the GFP/RFP protein framework. Remarkably, the GFP/RFP protein architecture promotes not only ring formation and fluorophore biosynthesis but also covalent bond cleavage at four consecutive positions along the polypeptide backbone,[25,40] trans−cis peptide bond isomerization,[41] decarboxylation chemistry,[24,25,42] oxidative side chain cross-links,[23] oxygen incorporation,[18] and now carbon−carbon cleavage chemistry (Scheme 1). Many of these amino acid modifications are likely driven by radical-based chemistry. The GFP/RFP protein scaffold achieves this diverse post-translational reactivity by favoring a particular backbone conformation for the chromophore-forming tripeptide, in which main chain atoms are unable to form

(35) Zhang, L.; Patel, H. N.; Lappe, J. W.; Wachter, R. M. *J. Am. Chem. Soc.* **2006**, *128*, 4766−4772.
(36) (a) Su, Q.; Klinman, J. P. *Biochemistry* **1998**, *37*, 12513−12525. (b) Mills, S. A.; Goto, Y.; Su, Q.; Plastino, J.; Klinman, J. P. *Biochemistry* **2002**, *41*, 10577−10584.
(37) Mills, S. A.; Klinman, J. P. *J. Am. Chem. Soc.* **2000**, *122*, 9897−9904.
(38) (a) Getzoff, E. D.; Tainer, J. A.; Weiner, P. K.; Kollman, P. A.; Richardson, J. S.; Richardson, D. C. *Nature* **1983**, *306*, 287−290. (b) Tainer, J. A.; Getzoff, E. D.; Richardson, J. S.; Richardson, D. C. *Nature* **1983**, *306*, 284−287.
(39) Heim, R.; Cubitt, A. B.; Tsien, R. Y. *Nature* **1995**, *373*, 663−664.
(40) (a) Quillin, M. L.; Anstrom, D. M.; Shu, X.; O'Leary, S.; Kallio, K.; Chudakov, D. M.; Remington, S. J. *Biochemistry* **2005**, *44*, 5774−5787. (b) Wilmann, P. G.; Petersen, J.; Devenish, R. J.; Prescott, M.; Rossjohn, J. *J. Biol. Chem.* **2005**, *280*, 2401−2404. (c) Mizuno, H.; Mal, T. K.; Tong, K. I.; Ando, R.; Furuta, T.; Ikura, M.; Miyawaki, A. *Mol. Cell* **2003**, *12*, 1051−1058.
(41) (a) Tubbs, J. L.; Tainer, J. A.; Getzoff, E. D. *Biochemistry* **2005**, *44*, 9833−9840. (b) Yarbrough, D.; Wachter, R. M.; Kallio, K.; Matz, M. V.; Remington, S. J. *Proc. Natl. Acad. Sci. U.S.A.* **2001**, *98*, 462−467. (c) Wall, M. A.; Socolich, M.; Ranganathan, R. *Nat. Struct. Biol.* **2000**, *7*, 1133−1138.
(42) Pletneva, N.; Pletnev, S.; Tikhonova, T.; Popov, V.; Martynov, V.; Pletnev, V. *Acta Crystallogr., Sect. D* **2006**, *62*, 527−532.

hydrogen bonds, and by burying positively charged Arg96 and negatively charged Glu222 near the chromophore (Figure 1A). Previously, we provided data that buried Glu222 and the lack of main chain hydrogen bonds drive a spontaneous peptide hydrolysis reaction, whereas Arg96 positive electrostatic interactions favored radical anion formation and subsequent decarboxylation.[25] We and others have provided data that Arg96 has a role in backbone cyclization, likely in deprotonation of the Gly67 amide nucleophile.[18,20,21] Remarkably, unlike most metal-containing systems that achieve one-electron oxidative chemistry, GFP appears to use positively charged Arg96 to facilitate controlled oxidative chemistry and drive amino acid modifications. The results and analyses presented here further suggest that negatively charged Glu222 assists in deprotonation of the residue 66 Cα atom, consistent with previous proposals,[20] and functions as a branchpoint control for partitioning between spontaneous post-translational carbon−carbon oxidation and unprecedented cleavage pathways. Together with previous studies, our results provide the groundwork for the design of proteins with novel catalytic or reporter self-modifications and reveal details for how the GFP/RFP protein environment controls PTM chemistry to simultaneously favor chromophore biosynthesis and disfavor alternative reactivity.

Methods

Mutagenesis and Protein Purification. Using the QuikChange method (Stratagene), we introduced the Y66F and Y66F R96A mutations into GFPhal (S65T F99S M153T V163A GFP) to make GFP variants with the Thr-Phe-Gly chromophore sequence (renamed TFG and TFG R96A, respectively). Likewise the S65A Y66F (and E222A) mutations were introduced into GFPsol (F64L S65T F99S M153T V163A) to make the AFG (and AFG E222A) variants. The resulting plasmids were transformed into BL21-CodonPlus(DE3)-RIL *Escherichia coli* cells (Stratagene), which were grown at 25 °C in 3 L batches. At an optical density of 0.5 at 600 nm, protein expression was induced with 0.2 mM isopropyl-β-D-thiogalactoside. The bacteria cells were pelleted 6−12 h later and frozen in liquid nitrogen until purification. Proteins were purified by modifying a published protocol[43] to incorporate HQ (26 mm × 30 cm) (PerSeptive Biosystems, Inc.) and S-100 (26 mm × 60 cm) (Pharmacia) columns.[44]

Crystal Structure Determination and Refinement. GFP variants were crystallized at protein concentrations of 8−12 mg/mL by vapor diffusion in hanging drops by modifying a published protocol.[5,44] Initial crystal clusters were crushed, serially diluted in a stabilizing mother liquor solution (50 mM Hepes pH 8.0, 50 mM $MgCl_2$, 19% polyethylene glycol 4000), and used as microseeds to grow large single crystals. Diffraction data were collected from crystals that were cryocooled in the gas stream from liquid nitrogen, immediately after immersion in the stabilizing solution plus 20% ethylene glycol. Data sets were collected at the Stanford Synchrotron Radiation Laboratory; TFG (λ = 0.9706 Å), TFG R96A (λ = 0.984 Å), and AFG (λ = 0.979 Å) on beamline 9-1 and AFG E222A (λ = 0.979 Å) on beamline 11-1. Data sets were indexed and reduced in the $P2_12_12_1$ space group with the *hkl* package,[45] and phases were determined by molecular replacement with AMoRe.[46] The search model was a refined 1.0 Å GFPsol structure, determined by molecular replacement from a previous GFP structure.[5] Difference electron density and omit maps were manually fit with the XtalView package[47] and refined in either CNS[48] or Shelx-97[49] against all the diffraction data, except for 5% used for R_{free} calculations.[50] All structures were superimposed using Sequoia.[51]

Acknowledgment. We thank M. G. Finn for critical reading and insightful comments on this manuscript. We also thank long-time colleagues C. D. Putnam and T. I. Wood for many stimulating scientific discussions. This work was supported by the La Jolla Interfaces in Sciences (D.P.B.), NIH GM19290 Postdoctoral Fellowships (D.P.B.), and NIH Grant RO1 GM37684 (E.D.G.). Portions of this research were carried out at the Stanford Synchrotron Radiation Laboratory, a national user facility operated by Stanford University on behalf of the U.S. Department of Energy, Office of Basic Energy Sciences. The SSRL Structural Molecular Biology Program is supported by the Department of Energy, Office of Biological and Environmental Research and by the National Institutes of Health, National Center for Research Resources, Biomedical Technology Program, and the National Institute of General Medical Sciences.

JA063983U

(43) Deschamps, J. R.; Miller, C. E.; Ward, K. B. *Protein Expression Purif.* **1995**, *6*, 555−558.
(44) Barondeau, D. P.; Kassmann, C. J.; Tainer, J. A.; Getzoff, E. D. *J. Am. Chem. Soc.* **2002**, *124*, 3522−3524.
(45) Otwinowski, Z.; Minor, W. *Macromol. Crystallogr., Part A* **1997**, *276*, 307−326.
(46) Navaza, L. *Acta Crystallogr., Sect. A* **1994**, *50*, 157−163.
(47) McRee, D. E. *J. Struct. Biol.* **1999**, *125*, 156−165.
(48) Brunger, A. T.; Adams, P. D.; Clore, G. M.; DeLano, W. L.; Gros, P.; Grosse-Kunstleve, R. W.; Jiang, J.-S.; Kuszewski, J.; Nilges, N.; Pannu, N. S.; Read, R. J.; Rice, L. M.; Simonson, T.; Warren, G. L. *Acta Crystallogr., Sect. D* **1998**, *54*, 905−921.
(49) Sheldrick, G. M.; Schneider, T. R. *Methods Enzymol.* **1997**, *277*, 319−343.
(50) Brunger, A. T. *Nature* **1992**, *355*, 472−474.
(51) Bruns, C. M.; Hubatsch, I.; Ridderstrom, M.; Mannervik, B.; Tainer, J. A. *J. Mol. Biol.* **1999**, *288*, 427−439.